Pt-Dumbbells in Ba_3Pt_2: Interplay of Geometric and Relativistic Effects on Pt–Pt Bonding

Andrey Karpov, Ulrich Wedig, and Martin Jansen

Max-Planck-Institut für Festkörperforschung, Heisenbergstraße 1, D-70569 Stuttgart, Germany

Reprint requests to Prof. Dr. Martin Jansen. E-mail: m.jansen@fkf.mpg.de

Z. Naturforsch. **59b,** 1387 – 1394 (2004); received August 16, 2004

Dedicated to Professor Hubert Schmidbaur on the occasion of his 70th birthday

Ba_3Pt_2 has been synthesized by reaction of a 3 : 2 mixture of Ba and Pt at 1223 K in argon, and characterized by single-crystal X-ray structure determination and electrical resistivity measurements. Ba_3Pt_2 crystallizes in the Er_3Ni_2 structure type (space group $R\bar{3}$ with $a = 962.40(6)$, $c = 1860.6(1)$ pm, $Z = 9$, $R(F)_{N'} = 0.063$, $N'(hkl) = 777$), and is isotypic to Ca_3Pt_2 and Sr_3Pt_2. The Pt atoms occur in pairs at a distance of 303 pm. According to the analysis of the Electron Localization Function and the Crystal Orbital Hamilton Population obtained from DFT band structure calculations, covalent bonding can be assumed in the Pt-dumbbells, although it is weaker in Ba_3Pt_2 than in Ca_3Pt_2. The peculiarities of the platinum compounds due to relativistic effects are elaborated by a comparison with theoretical results for Ca_3Pd_2. Ba_3Pt_2 exhibits metallic conductivity ($\rho_{270} = 0.7$ m$\Omega \cdot$cm), which is in accordance with band structure calculations.

Key words: Barium, Band Structure Calculation, Crystal Structure, Intermetallic Compound, Platinum

Introduction

Among all transition elements, gold and platinum are singled out with respect to their electron affinities which are as high as 2.31 eV (Au) and 2.13 eV (Pt) [1]. This peculiarity is commonly explained by a strong relativistic contraction of their 6s orbitals [2]. Chemically, the resulting pronounced driving force to complete their 6s shells gives evidence in a stabilization of the negatively charged ions, Au^- or Pt^{2-}, as it has been observed for CsAu [3], Cs_3AuO [4], $Cs_7Au_5O_2$ [5] or Cs_2Pt [6]. In this series, Cs_2Pt is particularly sensitive to ambient conditions, and its synthesis and characterization was rather demanding. Extending our search for platinide anions, we have recently managed to prepare BaPt [7]. However, in this compound the full charge separation has not been reached. Instead, Pt atoms have been found to build infinite one-dimensional covalently bonded homonuclear chains $^1_\infty[Pt]^-$, and BaPt has been assigned the first example of a Zintl-Klemm compound containing a negatively charged transition metal as a polyanionic component. Continuing our exploration of the Ba−Pt system, we have tried to decrease the Pt content, with the goal to obtain shorter Pt fragments. Here we report on the synthesis and characterization of Ba_3Pt_2, containing Pt-dumbbells. The bonding between the Pt atoms has been studied by band structure calculations and by analysing the Electron Localization Function (ELF) and the Crystal Orbital Hamilton Population (COHP).

Experimental Section

Synthesis

Materials utilized were Ba (99% Sigma-Aldrich Chemie GmbH, Germany), which was distilled twice at 1100 K in a dynamic vacuum of 10^{-9} bar, and Pt sponge (99.9% MaTeck Material-Technologie & Kristalle GmbH, Germany), which was dried and degassed before use at 673 K in a dynamic vacuum of 10^{-9} bar. The elements were weighed in the molar ratio 3 : 2 in an argon-filled glove box ($H_2O < 0.1$ ppm, $O_2 < 1$ ppm; M. Braun GmbH, Germany), and placed into a tantalum tube, which was sealed under argon with an arc welder. To prevent oxidation, the tantalum tube was encapsulated in a silica jacket, under argon. The reaction mixture was heated with a rate of 50 K/h to 1223 K, annealed at this temperature for two days, and then cooled down to room temperature with a rate of 10 K/h. The product was isolated and handled under strictly inert conditions (Schlenk technique or glove box).

0932–0776 / 04 / 1100–1387 $ 06.00

Structure determination

A shiny, black crystal of dimensions $0.15 \times 0.15 \times 0.2$ mm^3 was mounted in a glass capillary inside the glove box. Data were collected on a SMART-APEX CCD X-ray diffractometer (Bruker-AXS, Karlsruhe) at 293 K with graphite monochromated Mo-K_α radiation. The lattice parameters were determined by powder diffractometry. Semiempirical absorption correction (SADABS) [8] was applied. The structure was solved by direct methods and refined in full-matrix least squares ($R(F)_{N'} = 0.063$, $R_w(F^2)_{N'} = 0.1271$, $N'(hkl) = 777$, for 24 parameters refined) using the SHELXTL-2000 program package [9]. The largest residual maximum and minimum in the difference Fourier synthesis were 4.64 and $-3.12e^-/Å^3$, respectively.

Analyses

Metal element analyses were performed using a scanning electron microscope (XL 30 TMP, Philips, Holland, tungsten cathode, 25 kV), equipped with an integrated *EDAX*-EDX system (S-UTW-Si(Li)-detector). To measure hydrogen contamination, the sample was oxidized with V_2O_5 in an O_2 stream [10] and the evolved water titrated pulse-coulometric according to the *Karl Fischer* method [11].

Powder X-ray diffraction

In order to check for phase purity, the compound was examined by X-ray powder diffraction. Powder patterns were collected with a linear position-sensitive detector on a STADI P diffractometer (Stoe & Cie GmbH, Germany, Ge-monochromated Mo-$K_{\alpha 1}$ radiation, 2θ range $4-40$ degrees, step 0.01 degree). No extra reflections were observed compared to those calculated from atomic coordinates as determined by single crystal structure analysis, using the STOE Win XPOW software [12]. Lattice constants as determined from the powder data are $a = 962.40(6)$ and $c = 1860.6(1)$ pm.

Differential scanning calorimetry

Differential Scanning Calorimetry (DSC) was performed with a computer-controlled DSC sensor (DSC 404 C Pegasus, Netzsch GmbH, Germany). A powder sample (20 mg) was placed in a platinum crucible with a lid, heated to 1373 K with a rate of 10 K/min, and then cooled down to room temperature with the same rate. The whole process was run under argon.

Electrical resistivity

Temperature dependent resistivity has been obtained for a pressed pellet of Ba_3Pt_2 using the *van der Pauw* method [13]. Ba_3Pt_2 was ground into a powder and subsequently pressed into a 6 mm diameter by 1 mm thick pellet. The pellet was then connected to four probes of the resistivity measurement apparatus. A current of 10 mA (Keithley 2400 current source) was applied, and the voltage was measured with a Hewlett Packard 34420 nanovoltmeter in temperature range $5-290$ K at 5 K intervals.

Band structure calculations

DFT band structure calculations with the LDA functional of v. Barth and Hedin [14] were performed using the TB-LMTO-ASA program [15]. Scalar relativistic effects were considered when computing the partial waves. Empty spheres were added in order to achieve space filling [16].

Table 1. Crystallographic and technical data of single crystal structure refinement of Ba_3Pt_2[a].

Empirical formula	Ba_3Pt_2
Space group; Z	$R\bar{3}$ (no. 148); 9
Formula weight [g·mol^{-1}]	802.20
Lattice constants (powder data) [pm]	$a = 962.40(6)$, $c = 1860.6(1)$
Volume [10^6·pm^3]	1492.4(2)
$\rho_{calcd.}$ [g·cm^{-3}]	8.033
Data collection	Bruker-AXS, APEX-CCD SMART; Mo-K_α; ($\lambda = 71.073$ pm); Graphite monochromator; ω-mode
Temperature [K]	298
2θ Range [°]	5 – 56
Absorption correction	Semiempiric, SADABS [8]
Absorption coefficient μ [mm^{-1}]	59.43
Structure solution and refinement	Direct methods, least-squares refinement (F^2), SHELXTL-2000 [9]
No. of variables	24
Index range	$-12 \le h, k \le 12$, $-24 \le l \le 24$
N_{mes}; N(hkl); N'(hkl) with $I > 2\sigma(I)$	5237; 795; 777
R_{int}; $R(F)_N$; $R(F)_{N'}$	0.0518; 0.0643; 0.0628
$R_w(F^2)_N$; $R_w(F^2)_{N'}$; Goodness of fit	0.1276; 0.1271; 1.376
ΔF_{max}; ΔF_{min}/e·10^{-6}·pm^{-3}	4.64; −3.12
Weighting factors	$w_1 = 0$; $w_2 = 737.73$

[a] Further details of the crystal structure investigation are available from the Fachinformationszentrum Karlsruhe, D-76344 Eggenstein-Leopoldshafen (Germany), on quoting the depository number CSD-391284, the name of the author(s), and citation of the paper.

Table 2. Atomic coordinates and isotropic displacement parameters U_{eq}/pm^2 for Ba_3Pt_2[a].

		x	y	z	U_{eq}
Pt	18f	0.3103(1)	0.2488(1)	0.1020(1)	227(3)
Ba1	18f	0.0891(2)	0.4120(2)	0.0763(1)	184(4)
Ba2	6c	0	0	0.2029(1)	161(5)
Ba3	3a	0	0	0	206(8)

[a] U_{eq} is defined as one-third of the trace of the orthogonalized U_{ij} tensor.

Table 3. Anisotropic displacement parameters U_{ij}/pm^2 for Ba_3Pt_2.

	U_{11}	U_{22}	U_{33}	U_{23}	U_{13}	U_{12}
Pt	151(5)	201(5)	320(6)	−77(4)	21(4)	83(4)
Ba1	176(7)	175(7)	199(7)	15(6)	11(6)	86(6)
Ba2	135(7)	U_{11}	211(13)	0	0	68(4)
Ba3	198(11)	U_{11}	221(19)	0	0	99(6)

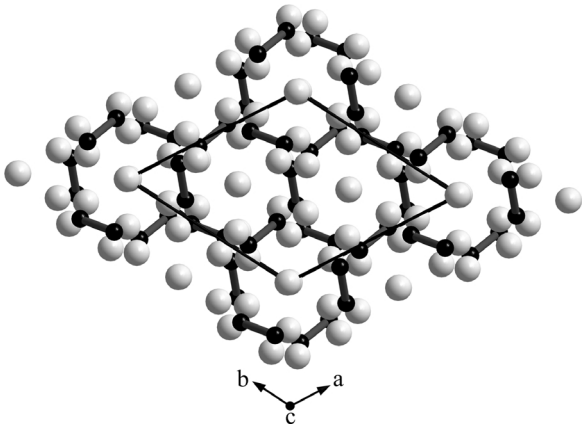

Fig. 1. View of the Ba_3Pt_2 structure along the c-axis showing pairs of Pt atoms (black dumbbells) separated by Ba atoms (light gray balls). Black lines mark the unit cell.

The Pt 5f, Ba 6p and 4f, and the 3d functions of the empty spheres were downfolded [17]. Atomic charges were obtained from a topological analysis of the electron density according to Bader [18]. Bonding properties were investigated both by analysing the Electron Localization Function (ELF) [19] and by calculating the Crystal Orbital Hamilton Population (COHP) [20]. The ELF results from a comparison of the local Pauli repulsion in the compound with that in an uniform electron gas of the respective electron density at a given point. It can take on values between 0 and 1. High ELF values are found in core shells, covalent bonds and lone pairs. The ELF and the basins resulting from the topological analysis of the electron density were calculated including core electrons. The charges within the basins were obtained by integrating the valence electron density in a regular mesh with 0.05 Å distance between the grid points. A detailed discussion of the interpretation of the ELF especially in transition metal compounds is published by Kohout *et al.* [21]. The ELF has proven to be a valuable tool to identify covalent substructures in intermetallic compounds [22].

Results and Discussion

Ba_3Pt_2 was synthesized by reaction from the elements at 1223 K in argon. According to the powder X-ray diffraction patterns, the product obtained is a single phase. The chemical composition was confirmed by EDX analysis, and no impurity elements were detected. The hydrogen impurity content amounts to 3 ± 1 at. % and thus can be neglected. The compound hydrolyses rapidly when exposed to air. According to DSC measurements, Ba_3Pt_2 melts at 1127 K. The electrical resistivity exhibits metallic-type temperature

Table 4. Selected interatomic distances/pm for Ba_3Pt_2.

Pt	–Pt	303.1(2)	Ba1	–Pt	325.1(2)
	–Ba2	314.9(1)		–Pt	326.8(2)
	–Ba1	325.1(2)		–Pt	334.9(2)
	–Ba1	326.8(2)		–Pt	343.1(2)
	–Ba2	332.0(2)		–Pt	365.3(2)
	–Ba3	333.2(1)		–Ba2	387.8(2)
	–Ba1	334.9(2)		–Ba3	388.2(2)
	–Ba1	343.1(2)		–Ba1	409.6(3)
	–Ba1	365.3(2)		–Ba1	413.4(3)×2
				–Ba1	416.1(3)×2
Ba2	–Pt	314.9(1)×3		–Ba2	431.3(2)×2
	–Pt	332.0(2)×3		–Ba2	453.5(3)
	–Ba3	377.5(3)		–Ba1	459.3(2)
	–Ba1	387.8(2)×3			
	–Ba1	431.3(2)×3	Ba3	–Pt	333.2(1)×6
	–Ba1	453.5(3)×3		–Ba2	377.5(3)×2
				–Ba1	388.2(2)×6

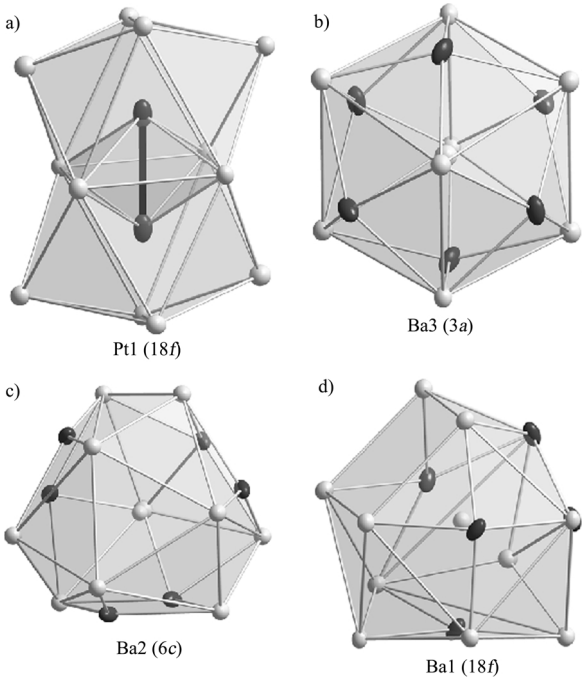

Fig. 2. Coordination polyhedra in ellipsoids representation of the four crystallographic distinct atoms in Ba_3Pt_2: a) Pt; b) Ba3; c) Ba2; d) Ba1 (probability factor 0.75; black – Pt atoms, light gray – Ba atoms). For Pt atoms a pair of interpenetrating polyhedra is shown.

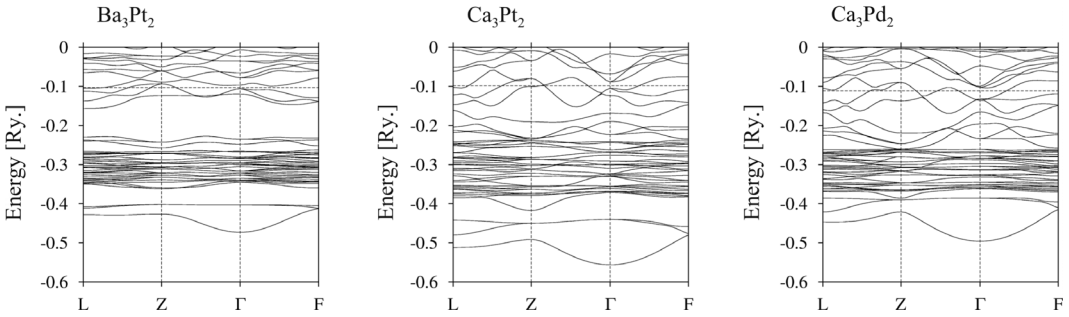

Fig. 3. LMTO-TB-ASA band structure of Ba_3Pt_2 (*left*), Ca_3Pt_2 (*middle*), and Ca_3Pd_2 (*right*).

dependence increasing from 0.45 m$\Omega \cdot$ cm at 5 K to 0.75 m$\Omega \cdot$ cm at 300 K.

Ba_3Pt_2 crystallizes in the Er_3Ni_2 structure type [23]. Tables 1 – 3 list crystallographic parameters obtained for a single crystal, while interatomic distances are given in Table 4. The Pt atoms occur in pairs at a distance of 303.3 pm (Fig. 1; Table 4). At slightly longer distances (315 – 365 pm), there are twelve Ba atoms, which separate the Pt-dumbbells from each other, so that the next Pt atoms occur at distances beyond 460 pm, only.

We describe the structural unit formed as a pair of rectangular face sharing trigonal prisms with the remaining four rectangular faces capped by barium (Fig. 2a). Ba3 atoms occupy sites with the highest possible symmetry of the structure (3*a*) and are coordinated by six Pt atoms (at 333 pm) in the first sphere, by six Ba2 atoms (at 378 pm) in the second sphere, and by two Ba1 atoms (at 388 pm) in the third sphere in a shape of rhombic dodecahedron (Fig. 2b). The coordination polyhedron around Ba2 atoms is the ideal 16-coordinated Frank-Kasper polyhedron [24] (Fig. 2c; Table 4). Ba1 atoms are surrounded by 16 neighbours in a shape of a very strongly distorted coordination polyhedron with one square face (Fig. 2d).

It is worthwhile to mention that a number of other AE_3T_2 compounds (AE = alkali-earth element, T = transition metal) crystallize in the same structure type. In Table 5 an overview of known AE_3T_2 compounds together with their crystal volumes per formula unit and T–T distances is given. In the row Ca–Sr–Ba a monotonously increase of the cell volumes is observed. For all compounds the formation of AE_3T_2 compounds is accompanied with a shrinking of volumes, as compared to the respective constituting elements. Surprisingly, a maximum for this contraction

Table 5. Volumes per formula unit and T–T distances for selected $(AE)_3T_2$ compounds.

Compound	$V_{cell}/Z/10^6$ pm^3	ΔV/%[a]	d(T–T)$_{A3T2}$/pm[b]	Δ d/%[c]
Ca_3Pd_2 [25]	129.9	−18.9	271 (275)	−1.45
Ca_3Pt_2 [26]	124.7	−22.5	268 (277)	−3.24
Sr_3Ag_2 [27]	177.7	−12.2	299 (289)	+3.46
Sr_3Au_2 [28]	163.0	−19.3	304 (288)	+5.56
Sr_3Pt_2 [26]	149.0	−24.9	284 (277)	+2.53
Ba_3Ag_2 [29]	200.6	−10.7	312 (289)	+7.96
Ba_3Au_2 [28]	184.2	−17.9	305 (288)	+5.90
Ba_3Pt_2, this work	165.8	−24.9	303 (277)	+9.39

[a] Volume change $\Delta V = 100 \times [V(AE_3T_2) - 3V(AE) - 2V(T)]/[3V(AE) + 2V(T)]$; [b] In parentheses d(T–T)$_T$ – metal-metal distances in elements are given [30]; [c] T–T distance change $\Delta d = 100 \times [d(T-T)_{A3T2} - d(T-T)_T]/[d(T-T)_T]$.

is observed for AE_3Pt_2 reaching 25% for Sr_3Pt_2 and Ba_3Pt_2. For Ca_3Pt_2 even a significant contraction of the Pt–Pt distance as compared to that in Pt metal [30] has been observed (Table 5). Moving to Sr and Ba compounds, the Pt atoms are pushed away from each other by their larger neighbours and the Pt–Pt distance increases to 303 pm for Ba_3Pt_2, nevertheless still being in a range where one can expect an interaction between the Pt atoms. The tendency of Pt atoms to build homonuclear fragments or chains is widely known. One of the prominent examples is Krogmann's salt $K_2[Pt(CN)_4]Cl_{0.33}$ with a columnar structure which is characterized by direct Pt–Pt contacts at a distance of 280 pm, mediated through d-orbitals overlapping [31].

To find out common features of the EA_3T_2 family on one hand and peculiarities of the platinum compounds on the other hand, band structure calculations were performed for Ba_3Pt_2, Ca_3Pt_2 and Ca_3Pd_2. In each of these cases, the band structure (Fig. 3) can be divided into 3 regions along the energy scale.

The lowest region below about -.4 Rydberg consists of 3 bands. For all three compounds the shapes

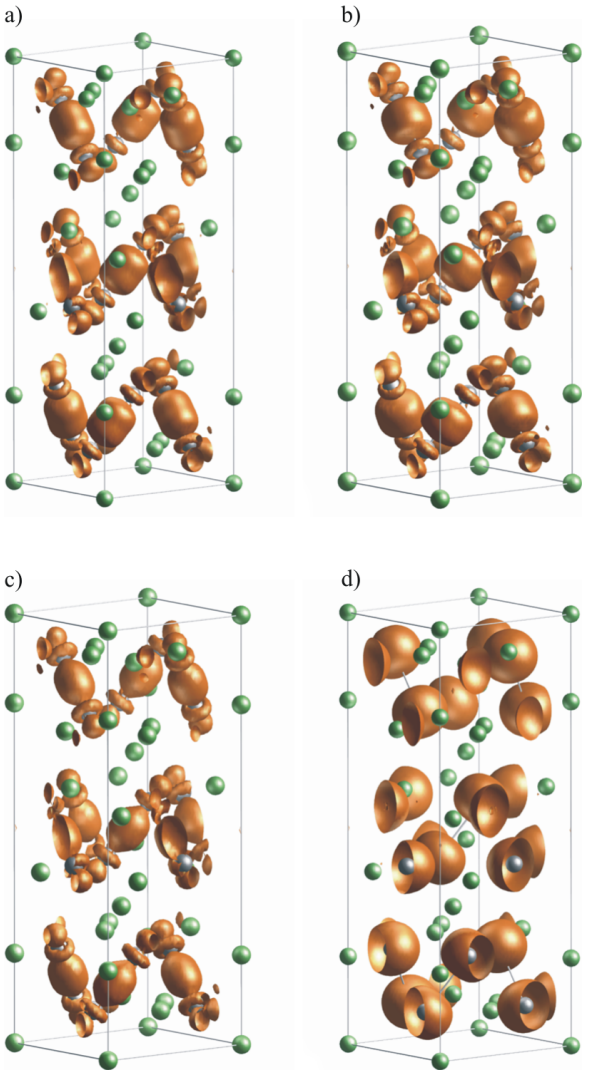

Fig. 4. Isosurfaces of the electron densities computed from the 3 lowest bands (*covalent region*): a) Ba_3Pt_2: $\rho = 0.01e^-/\text{Bohr}^3$; b) Ca_3Pt_2: $\rho = 0.01e^-/\text{Bohr}^3$; c) Ca_3Pd_2: $\rho = 0.01e^-/\text{Bohr}^3$; and from the bands 4 – 36 (*atomic region*): d) Ba_3Pt_2: $\rho = 0.05e^-/\text{Bohr}^3$.

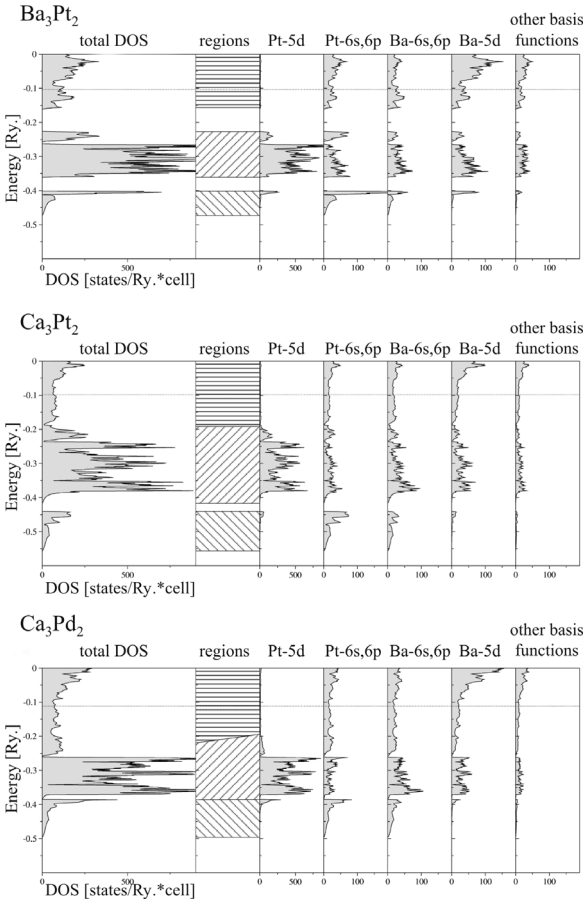

Fig. 5. Total and partial densities of states for Ba_3Pt_2 (*top*), Ca_3Pt_2 (*middle*), and Ca_3Pd_2 (*bottom*). For each compound, right to the total DOS, the subdivision of the energy range into 3 regions is represented: *covalent region* (lower), *atomic region* (middle), and *metallic region* (upper); see text.

of the electron density computed from these 3 bands look very similar (Fig. 4). They form the bonds within the transition element dumbbells. This energy region will be further on called *covalent region*.

The next 33 bands may also be grouped together. The partial densities of states presented in Fig. 5 show that they are basically built from the d-functions of the transition metal. As the calculations were performed for the rhombohedral cell containing 3 formula units, the 33 bands correspond to 11 electrons per transition metal atom which is more than needed to just fill the d-shell. Nevertheless this energy region in the band structure will be called *atomic region* as the electron density calculated from these bands is mainly located at the transition metal atom (Fig. 4d for Ba_3Pt_2). The valence bands above the *atomic region* up to the Fermi level and the conduction bands are combinations of basis functions of the alkaline earth atoms with non negligible contributions of the s- and p-functions of the transition metal. The energy region around the Fermi level will be named *metallic region*.

In all 3 compounds, these regions defined above exist but their interplay is quite different. In Ba_3Pt_2 all three are clearly separated by an energy gap. The *atomic region* is narrower than in the other compounds.

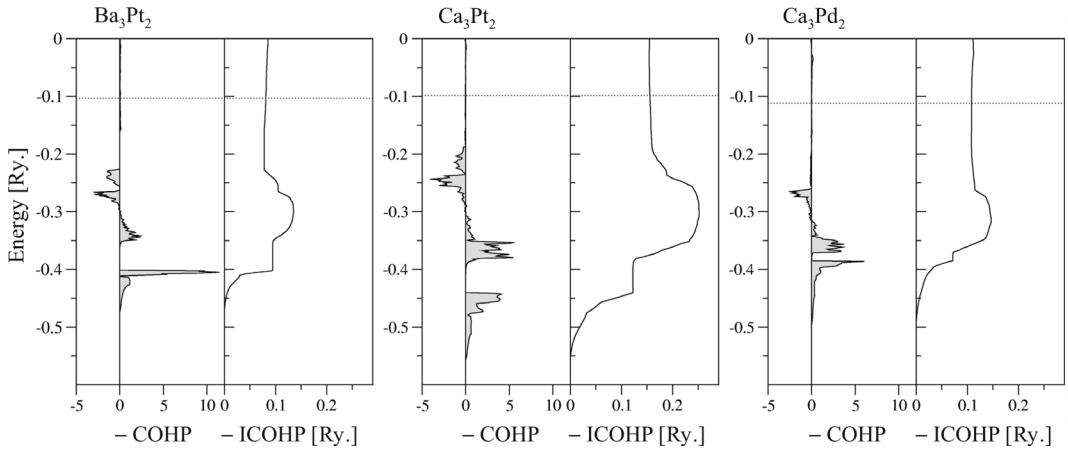

Fig. 6. Negative values of the Crystal Overlap Hamilton Population (-COHP) and the integral values (-ICOHP) for Ba_3Pt_2 (*left*), Ca_3Pt_2 (*middle*), and Ca_3Pd_2 (*right*). Note: Negative COHP values correspond to bonding contributions.

This points to a higher localization of the electrons. In Ca_3Pt_2 the gap between *metallic* and *atomic region* is closed, the latter being broadened considerably. In Ca_3Pd_2 both gaps are closed. Moreover the *atomic* and the *metallic regions* even have a significant overlap. Thus a distinction between these regions is no longer unambiguous.

The bands of the *covalent* and the *atomic region* altogether correspond to 72 electrons. If they all would be assigned to the transition metal, both Pd and Pt would have the oxidation state -2. The partial densities of states (Fig. 5), *e.g.* for the platinum s-, p- and d-functions in Ba_3Pt_2, however, integrate to a value of 59.1 electrons only, up to the top of the *atomic region*. The rest comes from contributions of the other basis functions. At this point it should be noted, that an analysis of the partial densities of states is not an investigation in terms of atomic orbitals but an analysis with respect to the basis functions. In the compounds discussed here, the atomic sphere radii, wherein the atom centred basis functions are defined, is restricted for the transition metal atoms by their distance within the dumbbells. Thus the radii of transition metal spheres is relatively small, compared to the alkaline earth radii. Moreover a considerable interstitial space is left, which has to be treated by basis functions within empty spheres, in the LMTO approach. With such a characteristic, basis set superposition effects are comparable to the real partial charges under discussion. A more basis set independent analysis of the charge distribution can be done by a topological analysis of the electron density and the subsequent integration of the valence electron density within the atomic basins [18]. The resulting partial charges for Pt and Pd respectively are: Ba_3Pt_2: -1.2; Ca_3Pt_2: -1.5; Ca_3Pd_2: -1.4. When discussing these numbers one should bear in mind, that the topological analysis just gives a criterion to subdivide the real space in the crystal. The numbers obtained by integration of the electron density within these basins contain no information about the character of the electrons, *e.g.*, whether they are more delocalized or whether they belong to some local ionic structure. However, the narrowness and the clear separation of the *atomic region* from the other regions as discussed above is an evidence for the more ionic character of platinum in Ba_3Pt_2.

Significant differences between the compounds can be seen when comparing the Crystal Orbital Hamilton Population (COHP, Fig. 6). The integrated values in the *covalent region* are smaller in Ba_3Pt_2 than in Ca_3Pt_2 due to the larger Pt–Pt distance. The contribution of the *atomic region* is of opposite sign. In Ca_3Pt_2 the Pt–Pt bond is strengthened, whereas in Ba_3Pt_2 an antibonding contribution results, which again shows the more local character of the *atomic region* in Ba_3Pt_2. In Ca_3Pd_2 the contribution of the *atomic region* is bonding like in Ca_3Pt_2. The bonding in the *covalent region* of Ca_3Pd_2 is significantly smaller although both calcium compounds have comparable bond lengths in the dumbbells. This may be attributed to a smaller s-contribution to the bands in the *covalent region* as can be seen in the partial DOSs, without however forgetting that an analysis of the partial DOSs is crucial for

these compounds. Another fact may support this hypothesis of different s-contributions to the T–T bonds. The Electron Localization Function (ELF) exhibits a maximum at the middle of the dumbbell, within the platinum compounds, although at rather low values (Ba_3Pt_2: $\eta = 0.273$; Ca_3Pt_2: $\eta = 0.296$). In Ca_3Pd_2 no maximum can be found at all. A larger contribution of the s-function to the Pt–Pt bonds can also be expected when regarding the radial extension of the atomic orbitals in the $nd^9(n+1)s^1$ configurations of Pt and Pd. The quotient of the r-expectation values ((n+1)s/nd) for Pt (1.7) is, due to the relativistic 6s-contraction, significantly smaller than for Pd (2.1) [32].

From the properties of the bands in the *covalent region*, we conclude that the bonding in the transition metal dumbbells is similar in both the Pt and the Pd compounds. While for Ca_3Pd_2 it is not necessary to consider relativistic effects in order to understand the bonding, the relativistic contraction of the 6s-orbital and, being connected with this, the high electron affinity of Pt, play an important role to stabilize the Pt–Pt bond over a wide distance rage. These effects allow a more flexible combination of s- and d-orbitals to form the appropriate bands and stabilize the more ionic atoms at larger distances. That's why the same structure type is found for compounds with the composition AE_3Pt_2 (EA = Ca, Sr, Ba), although the atomic radii of the alkaline earth elements as well as the Pt–Pt distance vary by more than 10%. To our knowledge, corresponding palladium compounds of Sr and Ba are still unknown.

Conclusions

A characteristic feature of the novel compound Ba_3Pt_2 is the occurrence of Pt atoms in pairs. The homonuclear Pt bonding is observed for a whole series of $(AE)_3Pt_2$ compounds, decreasing from AE = Ca to AE = Ba because of geometric constraints due to the overall 3-D structure. The existence of the same structure type with the three named alkaline earth elements, not yet observed for the lighter homologue Pd, is explained by effects, originating from the relativistic contraction of the s-orbitals in Pt. Ba_3Pt_2 exhibits metallic conductivity, which is in agreement with band structure calculations.

Acknowledgements

We gratefully acknowledge C. Mühle for his support at the experimental work, G. Siegle for resistivity measurements, R. Eger for hydrogen titration and the Fonds der Chemischen Industrie for continuous financial support.

[1] T. Andersen, H. K. Haugen, H. Hotop, J. Phys. Chem. Ref. Data **28**, 1511 (1999).
[2] P. Pyykkö, J. P. Desclaux, Acc. Chem. Res. **12**, 276 (1979).
[3] a) A. Sommer, Nature **152**, 215 (1943); b) W. E. Spicer, A. H. Sommer, J. G. White, Phys. Rev. **115**, 57 (1959).
[4] a) C. Feldmann, M. Jansen, Angew. Chem. **105**, 1107 (1993); Angew. Chem. Int. Ed. **32**, 1049 (1993); b) C. Feldmann, M. Jansen, J. Chem. Soc., Chem. Commun. 1045 (1994); c) A. Pantelouris, G. Küper, J. Hormes, C. Feldmann, M. Jansen, J. Am. Chem. Soc. **117**, 11749 (1995).
[5] a) A.-V. Mudring, M. Jansen, Angew. Chem. **112**, 3194 (2000); Angew. Chem. Int. Ed. **39**, 3066 (2000); b) A.-V. Mudring, J. Nuss, U. Wedig, M. Jansen, J. Solid State Chem. **155**, 29 (2000).
[6] A. Karpov, J. Nuss, U. Wedig, M. Jansen, Angew Chem. **115**, 4966 (2003); Angew. Chem. Int. Ed. **42**, 4818 (2003).
[7] A. Karpov, J. Nuss, U. Wedig, M. Jansen, J. Am. Chem. Soc. accepted.
[8] Sadabs: G. M. Sheldrick, Bruker AXS, Inc. Madison, USA, Bruker Nonius area detector scaling and absorption correction, SADABS Version 2.10 (2001).
[9] Shelxtl: G. M. Sheldrick, Bruker AXS, Inc. Madison, USA, Program package for crystal structure solution and refinement, SHELXTL Version 6.12 (2001).
[10] R. Eger, H. Mattausch, A. Simon, Z. Naturforsch. **48b**, 48 (1993).
[11] K. Fischer, Angew. Chem. **48**, 394 (1935).
[12] WinXPOW: Stoe & Cie GmbH, Darmstadt, Germany, Program package for operating with powder diffractograms, WinXPOW STOE Version 1.06 (1999).
[13] a) L. J. Van der Pauw, Philips Res. Rep. **13**, 1 (1958); b) J. P. Suchet, Electrical Conduction in Solid Materials, in B. R. Pamplin (gen. ed.): International Series of Monographs in the Science of the Solid State, Pergamon Press, Oxford (1975).
[14] U. Von Barth, L. Hedin, J. Phys. C **5**, 1629 (1972).
[15] TB-LMTO-ASA: R. W. Tank, O. Jepsen, A. Burkhardt, O. K. Andersen, Max-Planck-Institut für Festkörperforschung, Stuttgart, Germany, TB-LMTO-ASA Version 4.7 (1998).
[16] W. R. L. Lambrecht, O. K. Andersen, Phys. Rev. B **34**, 2439 (1986).
[17] O. K. Andersen, A. V. Postnikov, S. Yu. Savrasov, Mat. Res. Symp. Proc. **253**, 37 (1992).
[18] R. F. W. Bader, Atoms in Molecules: a Quantum Theory, Oxford University Press, Oxford (1990).
[19] a) A. Savin, A. D. Becke, J. Flad, R. Nesper,

H. Preuss, H. G. von Schnering, Angew. Chem. **103**, 421 (1991); Angew. Chem. Int. Ed. Engl. **30**, 409 (1991); b) A. Savin, O. Jepsen, J. Flad, O. K. Andersen, H. Preuss, H. G. von Schnering, Angew. Chem. **104**, 186 (1992); Angew. Chem. Int. Ed. Engl. **31**, 187 (1992).

[20] R. Dronskowski, P. E. Blöchl, J. Phys. Chem. **97**, 8617 (1993).

[21] M. Kohout, F. R. Wagner, Y. Grin, Theor. Chem. Acc. **108**, 150 (2002).

[22] a) Y. Grin, U. Wedig, H. G. von Schnering, Angew. Chem. **107**, 1318 (1995); Angew. Chem. Int. Ed. Engl. **34**, 1204 (1995); b) Y. Grin, U. Wedig, F. Wagner, H. G. von Schnering, A. Savin, J. Alloys Compd. **255**, 203 (1997).

[23] J. M. Moreau, D. Paccard, D. Gignoux, Acta Crystallogr. B **30**, 328 (1974).

[24] F. C. Frank, J. S. Kasper, Acta Crystallogr. **11**, 184 (1958).

[25] A. Palenzona, P. Manfrinetti, J. Less-Common Met. **85**, 307 (1982).

[26] A. Palenzona, J. Less-Common Met. **78**, P49 (1981).

[27] F. Merlo, M. L. Fornasini, Rev. Chim. Min. **21**, 273 (1984).

[28] M. L. Fornasini, F. Merlo, M. Pani, Rev. Chim. Min. **22**, 791 (1985).

[29] G. Bruzzone, M. Ferretti, F. Merlo, J. Less-Common Met. **128**, 259 (1987).

[30] P. Villars, L. D. Calvert, Pearson's Handbook Desk Edition; Crystallographic Data for Intermetallic Phases, ASM International (1997).

[31] a) K. Krogmann, Angew. Chem. **81**, 10 (1969); b) K. Krogmann, H. D. Hausen, Z. Anorg. Allg. Chem. **358**, 67 (1968).

[32] Computed with the scalar relativistic atomic code of the pseudopotential generation package of P. Giannozzi: http://www.nest.sns.it/∼giannozz.